Angular correlation functions of light scattered from weakly rough metal surfaces

C. S. West* and K. A. O'Donnell†
The School of Physics, Georgia Institute of Technology, Atlanta, Georgia 30332
(Received 23 July 1998)

The angular correlation functions of light diffusely scattered from weakly rough metal surfaces are studied. In experimental work, surfaces are well characterized, have highly one-dimensional roughness, and are studied in the case of *p* polarization. If there is significant plasmon polariton excitation, one type of intensity correlation function indicates that the diffuse intensity decorrelates rapidly as the angle of incidence is varied. It exhibits peaks that arise from an autocorrelation of identical intensities, or from the correlation of intensities related by the reciprocity principle. A second intensity correlation function expresses the symmetry of the diffuse intensity about the specular direction and is significant without plasmon polariton excitation. It is shown that the intensity correlation functions are directly related to two fundamental amplitude correlation functions. The latter are studied with perturbation theory, including all terms to fourth order in the surface profile function. The relation of the observed effects to backscattering enhancement is thus established, and favorable comparisons are made with the experimental results. [S0163-1829(99)05103-6]

I. INTRODUCTION

The scattering of light from randomly rough surfaces has attracted attention over the years. Of considerable interest is the case of a weakly rough metal surface, for which the standard deviation of surface height σ is much less than the illumination wavelength λ. Here, not only may the random roughness allow an incident light wave to launch surface plasmon polaritons, but it also may scatter the excited plasmon polaritons, thus transforming them into diffuse light escaping from the surface. If these scattering processes are significant, it is well known that backscattering enhancement may appear.[1] The effect is apparent, in the mean diffusely scattered intensity, as a peak in the direction of retroreflection. The peak arises from constructive interference and has seen a sustained level of interest, with many theoretical studies applying either perturbation theory[2–10] or numerical methods.[11] This type of backscattering peak was first observed recently;[12,13] the delay is due largely to the difficulties encountered in the microlithographic fabrication of rough surfaces producing sufficient plasmon polariton excitation.

In addition to the mean intensity, the correlation functions associated with the diffuse scatter have also been of interest. We ask the following: when will the amplitudes (or intensities) scattered into the far field for different incident and scattering angles be correlated with one another, and what form will these correlation functions take? For weakly rough surfaces, this question has been addressed through theoretical study of the angular correlation functions of scattered amplitude,[14] where it was claimed that the same constructive interference producing backscattering enhancement also appears in these correlation functions. Other theoretical works have considered the correlation functions of intensity,[15–17] which were found to contain contributions arising from a wide variety of plasmon polariton-related scattering processes. Generally speaking, it was shown that these correlation functions contain much more detailed information about the dominant scattering processes than does the mean diffuse intensity.

Despite this theoretical interest, there has been a complete lack of experimental studies of these important correlation functions in the case of weak roughness. Because the scattered intensity is readily detected while the amplitude is not, our first purpose here is thus to present measurements of the intensity correlation functions. We show results for two gold surfaces for which σ is of the order of 10 nm, but the surfaces have quite different power spectra. Thus, one surface produces little plasmon polariton excitation, but the second exhibits strong scattering contributions associated with these surface waves. These two surfaces produce intensity correlation functions of quite diverse character and serve to illustrate a broad range of behavior. We then draw comparisons with previous theoretical works by considering the various predicted contributions to the intensity correlation functions.

Our second purpose is to present a theoretical interpretation of the results. In the limit of large illuminated surface area, we first discuss that a Gaussian moment theorem allows the intensity correlation functions to be expressed in terms of two amplitude correlation functions. Because the amplitude correlations are of lower statistical order, we consider them to be more fundamental. These are evaluated using perturbation theory based on the reduced Rayleigh equations, including all terms to fourth order in σ. It is shown that the calculations are qualitatively (and, in some cases, quantitatively) consistent with the experimental measurements.

This introduction would be incomplete without recognizing parallel studies of angular correlation functions made in two other fields. First, in the case of a strongly rough surface with σ comparable to λ, the interest in angular correlations goes back many years[18–20] (see Fig. 10 of Ref. 18 for early examples of the memory effect discussed below). Much of this original interest was stimulated by the possibility of determining σ directly from measured angular correlations.[20] More recently, other papers have investigated the correlation functions when multiple scattering occurs within deep surface valleys.[21–24] Even though backscattering enhancement may arise from this type of multiple scattering, it is unrelated to polariton excitation; such works should thus be considered

as quite distinct from polariton-related studies with $\sigma \ll \lambda$.

There has also been much research on the light diffusely scattered from small particles. If multiple scattering is significant, the diffuse light may exhibit a backscattering peak.[25] The peak arises from constructive interference as do the surface effects and has been related to weak Anderson localization.[26] It was predicted that three different types of intensity correlations should exist,[27] which stimulated a number of theoretical[28] and experimental[29] investigations. Some of the correlations have been dubbed ''memory effects,'' for they reflect the manner in which the structure of the scattered field is remembered as the angle of incidence is changed. These correlation functions have some analogs in results to be presented here; it could be said that our results represent memory effects for weakly rough metal surfaces.

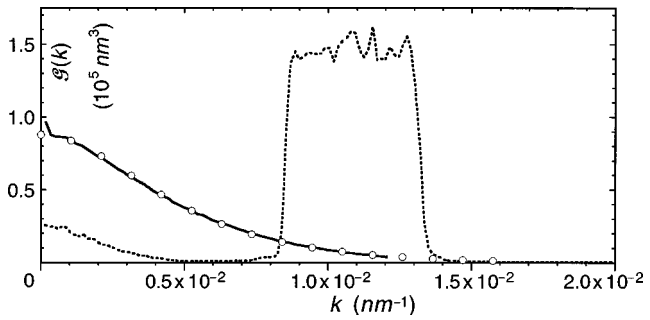

FIG. 1. For positive k, the measured power spectrum $\mathcal{G}(k)$ of the surface roughness for surface A (solid curve) and surface B (dotted curve). Circles denote the spectral model of Eq. (28) for surface A. Normalization is such that $2\pi\sigma^2$ is $\int_{-\infty}^{\infty}\mathcal{G}(k)dk$.

II. EXPERIMENTAL TECHNIQUES

One of the most challenging aspects of the experimental work was the fabrication of suitable rough surfaces. Care was taken to ensure that the roughness was highly one-dimensional, as is often assumed in calculations. Briefly, two 50×50-mm glass plates were coated with a 1.5-μm layer of Shipley S1400-27 photoresist. The first plate (plate A) was processed in a manner so as to produce a Gaussianlike power spectrum centered on zero wave number. In particular, a beam from a HeCd laser of wavelength $\lambda=442$ nm was expanded to approximately 150 mm diameter and was then incident on an opal glass. In the transmitted scatter, a photoresist plate was mounted in a plane parallel to the opal glass where finely-scaled speckle was present. As the plate was exposed, a motorized translation stage scanned the plate by 0.25 mm in a direction perpendicular to the normal of the opal glass. Thus, the time-integrated exposure was highly one-dimensional. Because any point of the plate received exposure from a large number of independent speckles, the statistics of the exposure should be consistent with a Gaussian random process.

The second plate (plate B) was processed in a manner so as to produce a roughness power spectrum of a displaced rectangular form.[12] It was exposed to 500 sinusoidal intensity distributions arising at the intersection of two light beams from the HeCd laser. Each sinusoidal pattern had a different spatial wave number k in the direction along the plate and was randomly phased with respect to other exposures. The minimum and maximum wave numbers ($k_{\min}=8.56\times10^{-3}$ nm^{-1} and $k_{\max}=1.33\times10^{-2}$ nm^{-1}, respectively) were well known from the exposing geometry. With the pattern wave numbers evenly spaced between $k_{\min}$ and $k_{\max}$ the net exposure behaves as a Fourier series that, for a large number of exposures, becomes consistent with a Gaussian random process.[12] The desired one-dimensionality follows from alignment of the sinusoidal exposing intensities.

Both plates were developed in a manner found to produce a linear relation between exposure and resulting surface height (30 sec in Shipley 352 developer). Using standard vacuum evaporative coating techniques, the samples were then coated with a thick layer (200 nm) of gold at a pressure less than 10^{-6} Torr. Efforts were also made to characterize the samples. We have found previously that samples made in the manner of sample A produce a mean diffuse intensity closely consistent with lowest-order perturbation theory. The lowest-order term depends directly on the surface power spectrum;[4] we have thus inverted the relation to determine the spectrum from a diffuse intensity measurement. Surface B, however, produces scatter quite different from lowest-order theory, so that the surface was characterized directly with a Talystep stylus profilometer. The roughness spectra $\mathcal{G}(k)$ are shown in Fig. 1. It can be seen that surface A has a Gaussianlike spectrum while, apart from low levels of spectral power for small k, the spectrum of surface B is well-constrained between $k_{\min}$ and $k_{\max}$. From the area of $\mathcal{G}(k)$, we determine σ to be 12.1 and 15.5 nm for surfaces A and B, respectively.

The high degree of roughness one dimensionality was apparent upon reflection of a laser beam from the samples. With the incident beam directed perpendicular to the grooves of the rough surface, the scattered light presented a one-dimensional speckled structure that was well-confined to the plane of incidence. Further, for an incident p or s polarization state, the diffuse scatter was identically polarized; we restrict all discussions here to p polarization because the scatter may then exhibit polariton-related effects.

We now briefly present typical measurements of these one-dimensional scattering distributions. Results are expressed as a mean diffuse intensity $\langle I(q|k)\rangle$ that represents scattered power per radian for unit incident power. Here $k=(\omega/c)\sin\theta_i$ and $q=(\omega/c)\sin\theta_s$, where ω is the frequency, and θ_i and θ_s are, respectively, the angles of incidence and scattering. This notation is used for consistency with theoretical development of Secs. IV and V. The angle brackets indicate an ensemble average to remove speckle noise that, in the experiments, was approximated by integrating the detector signal as the surface was spatially scanned. The sources used were an orange HeNe laser ($\lambda=612$ nm) or a semiconductor laser ($\lambda=674$ nm). The normalization of $\langle I(q|k)\rangle$ was obtained directly by measuring the incident beam with the detector.

Figure 2 shows $\langle I(q|k)\rangle$ in p polarization for several cases. Surface A produces a broad distribution that, surrounding the specular angle ($\theta_s=\theta_i$), resembles the shape of $\mathcal{G}(k)$ in Fig. 1. Indeed, $\mathcal{G}(k)$ was determined from this data as discussed earlier. In the case of surface B for $\lambda=612$ nm, the scatter for small $|\theta_s|$ arises almost entirely from plasmon polariton coupling; the narrow bandwidth of $\mathcal{G}(k)$ produces

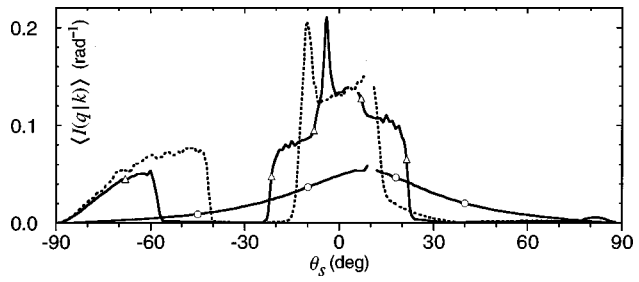

FIG. 2. Mean-diffuse intensities $\langle I(q|k)\rangle$ of surface A for $\lambda=612$ nm and $\theta_i=10°$ (solid curve, circles), surface B for $\lambda=612$ nm and $\theta_i=10°$ (dotted curve), and surface B with $\lambda=674$ nm and $\theta_i=4°$ (solid curve, triangles). Specular reflections are not shown; the total diffuse powers range from 0.0575 (surface A) to 0.112 (surface B, $\lambda=612$ nm).

strong lowest-order scatter only for $\theta_s<-42°$ in Fig. 2. In particular, $\mathcal{G}(k)$ has been designed so that for $\theta_i=\theta_{\max}=13°$, one may excite counterpropagating plasmon polaritons as

$$+k_{sp}=(\omega/c)\sin\,\theta_i+k_{\min} \tag{1a}$$

and

$$-k_{sp}=(\omega/c)\sin\,\theta_i-k_{\max}, \tag{1b}$$

where $\pm k_{sp}=\pm(\omega/c)\sqrt{\epsilon_1/(\epsilon_1+1)}$ is the wave number of a plasmon polariton traveling to the right $(+)$ or left $(-)$, $\epsilon=\epsilon_1+i\epsilon_2$ is the dielectric constant, and we estimate that $k_{sp}\cong 1.06\omega/c$. It is readily verified that for $|\theta_i|\leqslant\theta_{\max}$ as in Fig. 2, counterpropagating plasmon polaritons are launched because Eqs. (1) are satisfied for the roughness wave numbers in $\mathcal{G}(k)$ between $k_{\min}$ and $k_{\max}$. Now, $+k_{sp}$ and $-k_{sp}$ may themselves be scattered by the roughness, to be outwardly coupled as in

$$(\omega/c)\sin\,\theta_s=+k_{sp}-k_r \tag{2a}$$

and

$$(\omega/c)\sin\,\theta_s=-k_{sp}+k_r', \tag{2b}$$

where k_r and k_r' are roughness wave numbers available in $\mathcal{G}(k)$. It is easily shown that the rectangular part of $\mathcal{G}(k)$ constrains the outward coupling to $|\theta_s|\leqslant\theta_{\max}$, thus producing the central distribution of Fig. 2. It is the interference between the distinct processes involving $+k_{sp}$ and $-k_{sp}$ that produces the backscattering peak at $\theta_s=-\theta_i$. For the other case of Fig. 2 with $\lambda=674$ nm, the distributions associated with $+k_{sp}$ and $-k_{sp}$ shear apart from one another,[13] but the backscattering peak still appears for $\theta_i=4°$, as shown.

The following procedure was used to measure the angular correlation functions. The p-polarized laser beam was spatially filtered and focused to a waist on the surface. The illumination width w ($1/e$ diameter of the intensity) was 67 or 53 μm for $\lambda=612$ or 674 nm, respectively. The sample was mounted on a rotation stage to set θ_i; an arm mounted on a concentric rotation stage was used to record the intensity present at scattering angle θ_s. On this arm, in the far field 70 cm from the rough surface, was a slit of width 130 μm. All light entering the slit was collected by a field lens and was focused onto a silicon photodetector. The angle subtended by the slit was much smaller than the speckle width λ/w, so that integration effects should be negligible. We estimate that any systematic alignment errors in θ_i and θ_s were of the order of 0.01° and were also small compared to λ/w.

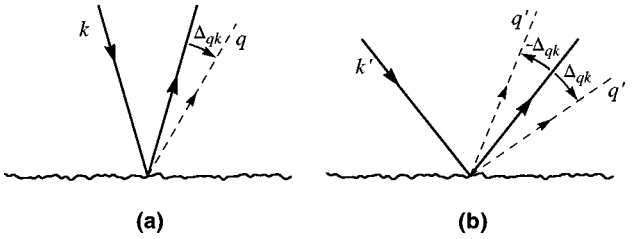

FIG. 3. Interpretation of the correlation conditions; solid outgoing rays denote the specular direction. An intensity for (q,k) may be correlated with an intensity for (q',k') that has deviation of magnitude $\Delta_{qk}=(q-k)$ to the right or left of the specular reflection.

To take a data set, a computer rotated the sample and detector stages to coordinates (θ_i,θ_s) and recorded the intensity detected. In a direction transverse to the incident beam, the sample was moved just sufficiently to cause the intensity to decorrelate, and the new intensity was recorded. This process was repeated until the uniform area of the rough surface had been fully utilized. After saving the data set to a disk file, further such data were taken for all other desired angle pairs (θ_i,θ_s). The process required considerable time to complete (3–5 days) and all correlations between files were then computed; three such data sets were taken.

Because it was impractical to do exhaustive searches for correlations, the following considerations dictated our approach. For one-dimensional roughness the lowest-order scattered amplitude for (q,k) is proportional to $\hat{\zeta}(q-k)$, where $\hat{\zeta}$ is the Fourier transform of the surface profile function.[4] First, one could expect a correlation between intensities at (q,k) and (q',k') if $(q'-k')=\Delta_{qk}'$ is identical to $(q-k)=\Delta_{qk}$, because $\hat{\zeta}$ is evaluated at the same coordinate to produce both amplitudes. Second, one may also expect an intensity correlation for $\Delta_{qk}'=-\Delta_{qk}$; the Fourier transform of the real surface profile is Hermitian, and the two scattered amplitudes are related because $\hat{\zeta}(q-k)=\hat{\zeta}^*(q'-k')$. These conditions are illustrated in Fig. 3. For the conditions (q,k), Δ_{qk} is the deviation from specularity $(q=k)$ and we employ a small value away from specular glare. Upon changing the illumination to condition k', the above arguments imply that we may find a correlated intensity either at position q' with identical deviation from specular (i.e., $q'=k'+\Delta_{qk}$), or else at a second q' equally displaced to the other side of specular (at $q'=k'-\Delta_{qk}$). In Sec. III, results may be visualized by choosing (q,k) in Fig. 3(a) and then plotting the correlation as k' varies, with it being understood that q' follows one of the two correlated directions in Fig. 3(b).

The general correlation function may be expressed as

$$C_{\Delta I}(q,k|q',k')=\langle\Delta I(q|k)\Delta I(q'|k')\rangle, \tag{3}$$

where $\Delta I=I-\langle I\rangle$. The first type of correlation function discussed is represented by

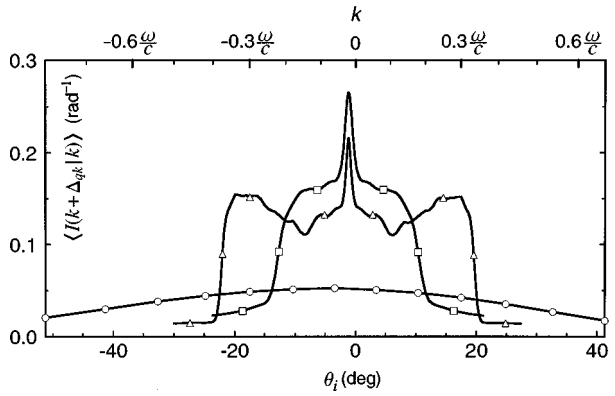

FIG. 4. Mean-diffuse intensities $\langle I(k+\Delta_{qk}|k)\rangle$ computed from averages of the data. Cases shown are surface A with $\lambda=612$ nm (circles), surface B with $\lambda=612$ nm (squares), and surface B for $\lambda=674$ nm (triangles).

$$C^{+}_{\Delta I}(k,k',\Delta_{qk})=C_{\Delta I}(k+\Delta_{qk},k|k'+\Delta_{qk},k'), \qquad (4)$$

while the second type is given by

$$C^{-}_{\Delta I}(k,k',\Delta_{qk})=C_{\Delta I}(k+\Delta_{qk},k|k'-\Delta_{qk},k'). \qquad (5)$$

We also find it useful to present the statistically normalized correlation functions

$$\rho^{\pm}_{\Delta I}(k,k',\Delta_{qk})=\frac{C^{\pm}_{\Delta I}(k,k',\Delta_{qk})}{\sqrt{\langle\Delta I^2(q|k)\rangle\langle\Delta I^2(q'|k')\rangle}}, \qquad (6)$$

where $0\leqslant|\rho^{\pm}_{\Delta I}|\leqslant 1$.

III. EXPERIMENTAL RESULTS

Data sets were taken for surface A with $\Delta_{qk}=\pm 0.12\omega/c$ and $\lambda=612$ nm, and for surface B with $\Delta_{qk}=\pm 0.04\omega/c$, with wavelengths either 612 or 674 nm. For each pair (θ_i,θ_s), 1.2×10^4 and 5.1×10^3 nearly independent intensities were measured for surfaces A and B, respectively, to compute the correlation functions. The number of angle pairs was 26 for surface A, and 170 and 262 for surface B with $\lambda=612$ and 674 nm, respectively. In the latter two cases, data are too dense to be plotted distinctly in the forthcoming figures. Throughout results the intensity is normalized as in Fig. 2; the resulting correlation units are rad^{-2}. All statistical error bars shown are computed directly from moments of the data and extend to plus or minus one standard deviation.

The mean intensities $\langle I(q|k)\rangle$ computed by averaging data sets for positive Δ_{qk} are shown in Fig. 4. As had been noted in Fig. 2, surface A produces a broad distribution without distinct features, while surface B produces a more compact distribution having a backscattering peak at both wavelengths. The peak falls at $q=-k$; because of the relation between q and k this occurs for $k=-\Delta_{qk}/2$, or thus at $\theta_i=-1.1°$ for surface B. The steep slopes from polariton excitation are obvious for surface B and, as plotted in Fig. 4, they appear symmetrically about the backscattering peak.

Correlation functions for surface A are shown in Figs. 5 and 6 with $\lambda=612$ nm. In Fig. 5, it is seen that $C^{+}_{\Delta I}(k,k',\Delta_{qk})$ and $C^{-}_{\Delta I}(k,k',\Delta_{qk})$ present broad curves centered near $\theta_i'=0°$. The slow decay arises largely from the

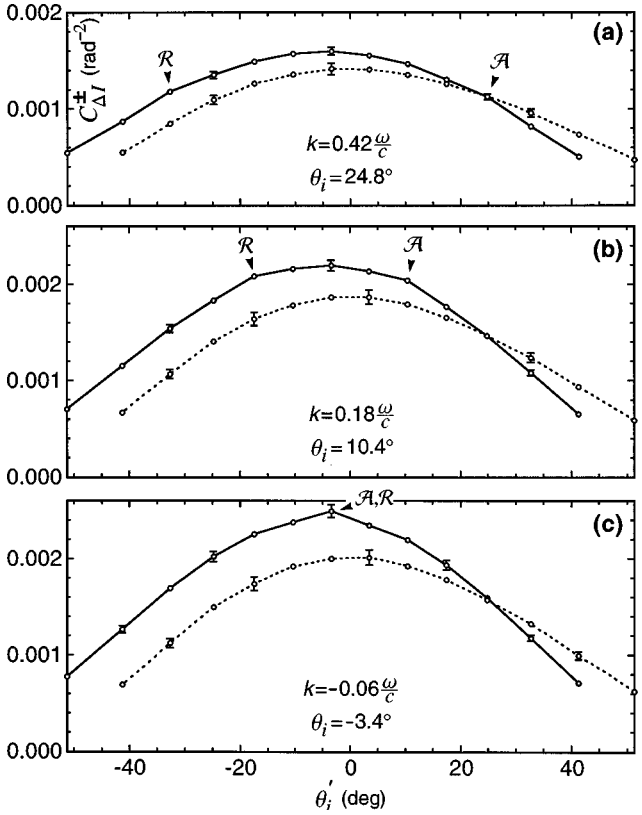

FIG. 5. Correlation functions $C^{+}_{\Delta I}(k,k',\Delta_{qk})$ (solid lines) and $C^{-}_{\Delta I}(k,k',\Delta_{qk})$ (dashed lines) for surface A, $\lambda=612$ nm, and $\Delta_{qk}=0.12\omega/c$. The autocorrelation ($\mathcal{A}$) and reciprocal ($\mathcal{R}$) points are indicated.

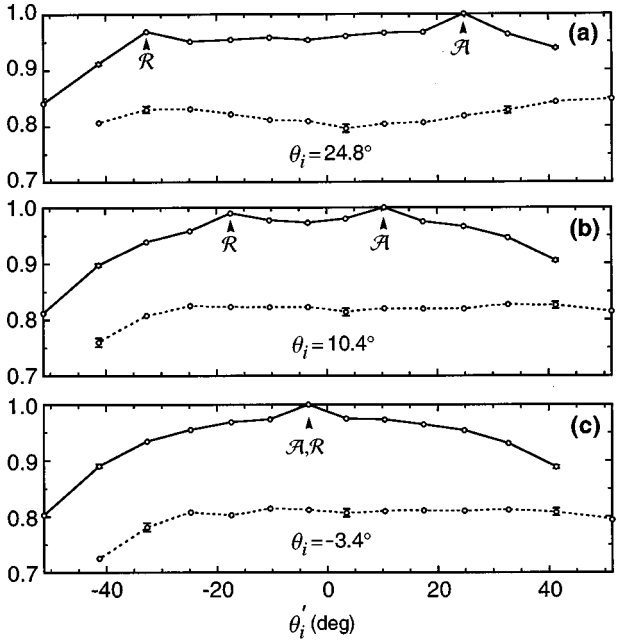

FIG. 6. Correlation functions $\rho^{+}_{\Delta I}(k,k',\Delta_{qk})$ (solid lines) and $\rho^{-}_{\Delta I}(k,k',\Delta_{qk})$ (dashed lines) for surface A, $\lambda=612$ nm, and $\Delta_{qk}=0.12\omega/c$. The autocorrelation ($\mathcal{A}$) and reciprocal ($\mathcal{R}$) points are indicated.

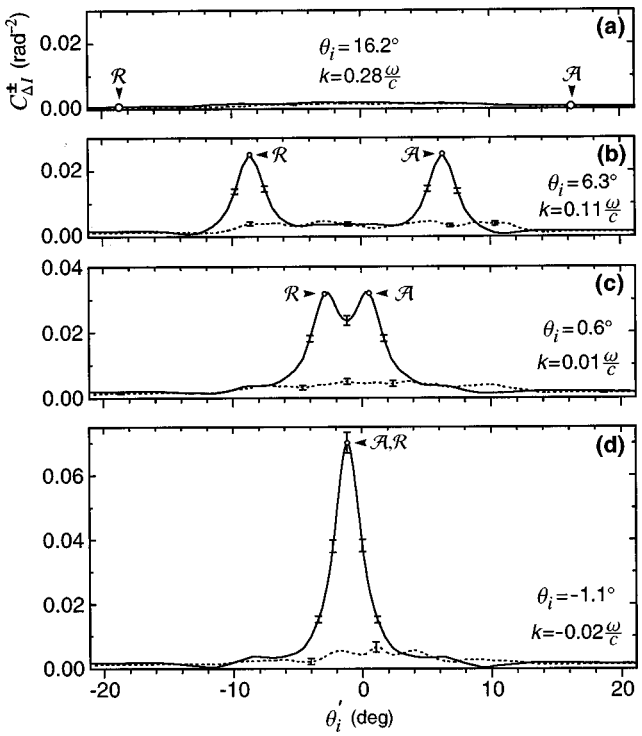

FIG. 7. Correlation functions $C^{+}_{\Delta I}(k,k',\Delta_{qk})$ (solid lines) and $C^{-}_{\Delta I}(k,k',\Delta_{qk})$ (dashed lines) for surface *B*, λ=612 nm, and $\Delta_{qk}=0.04\omega/c$. The autocorrelation ($\mathcal{A}$) and reciprocal ($\mathcal{R}$) peaks are apparent in (b)–(d).

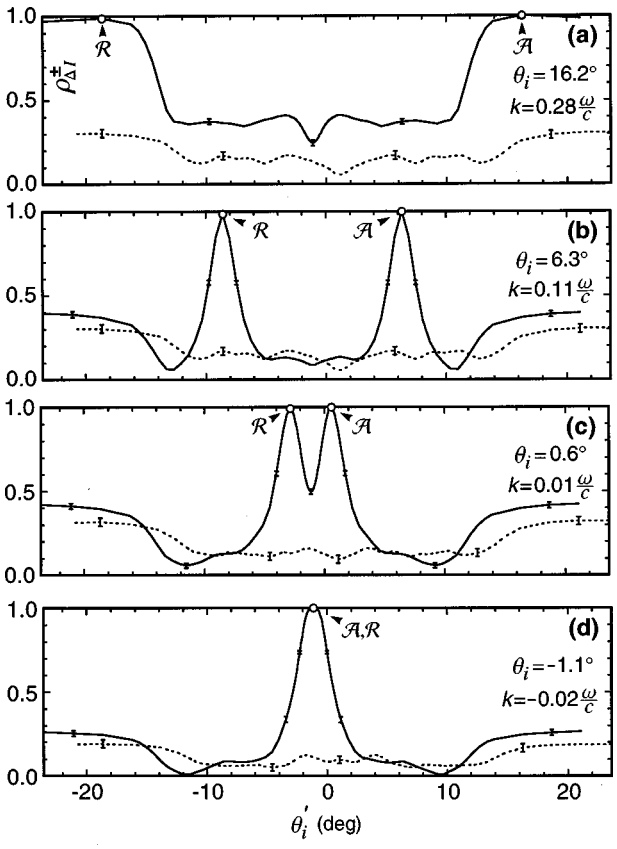

FIG. 8. Correlation functions $\rho^{+}_{\Delta I}(k,k',\Delta_{qk})$ (solid lines) and $\rho^{-}_{\Delta I}(k,k',\Delta_{qk})$ (dashed lines) for surface *B*, λ=612 nm, and $\Delta_{qk}=0.04\omega/c$. The autocorrelation ($\mathcal{A}$) and reciprocal ($\mathcal{R}$) points show essentially perfect correlation.

fall of the mean intensity; this is clear because $\rho^{+}_{\Delta I}(k,k',\Delta_{qk})$ and $\rho^{-}_{\Delta I}(k,k',\Delta_{qk})$ as shown in Fig. 6 remain strong, indicating little actual decorrelation. Throughout Fig. 6, $\rho^{+}_{\Delta I}$ contains a peak of unit height at $k'=k$ that represents an autocorrelation between identical intensities. In addition, a second peak arises from reciprocity; the reciprocity principle[30] states that reversing the incident and scattered wave vectors produces an identical scattered amplitude. Here, an amplitude for (q,k) must then be identical to another with $(q',k')=(-k,-q)$.[4] The two intensities correlated in $\rho^{+}_{\Delta I}$ are such a reciprocal pair for $k'=-k-\Delta_{qk}$, producing the second peak Figs. 6(a) and 6(b). Further, the case of Fig. 6(c) shows but a single peak, which appears where the autocorrelation and reciprocal conditions are simultaneously satisfied at backscattering with $k'=k=-\Delta_{qk}/2$. In the case of $\rho^{-}_{\Delta I}$ no distinct peaks appear, but $\rho^{-}_{\Delta I}$ remains near 0.8 and thus represents a significant and persistent correlation.

The correlation functions of surface *B* take different forms as shown in Figs. 7 and 8 with λ=612 nm. In Fig. 7(a), k is outside of the polariton coupling region of Fig. 4 and $C^{\pm}_{\Delta I}(k,k',\Delta_{qk})$ remains small for all θ_i'. However, the low levels of intensity nonetheless exhibit correlations; Fig. 8(a) shows that $\rho^{+}_{\Delta I}$ is strong outside of the coupling region, but decays within it, and decays further when the intensity at k' falls within the backscattering peak. In the other three cases $I(q/k)$ has strong polariton coupling; $C^{+}_{\Delta I}$ in Figs. 7(b) and 7(c) exhibits narrow peaks surrounding the autocorrelation and reciprocal points, with low levels elsewhere. In Fig. 7(c) the two peaks are interacting with one another and, in Fig. 7(d), they coincide when $I(q|k)$ is at backscattering. In Figs. 8(b)–8(d), $\rho^{+}_{\Delta I}$ exhibits peaks related to those of $C^{+}_{\Delta I}(k,k',\Delta_{qk})$ and demonstrates nearly perfect correlation at points where the two intensities are related by the reciprocity principle. Both $\rho^{+}_{\Delta I}$ and $\rho^{-}_{\Delta I}$ exhibit modest values outside of the polariton coupling region, but generally $\rho^{-}_{\Delta I}$ and $C^{-}_{\Delta I}$ remain small.

The results of Figs. 5–8 do little justice to the quantity of data taken, and, to accentuate the differences between surfaces *A* and *B*, we provide more complete plots of $C^{\pm}_{\Delta I}(k,k',\Delta_{qk})$ in Fig. 9. For $C^{+}_{\Delta I}$ in the case of surface *A*, Fig. 9(a) shows a broad envelope and thus indicates that the speckles generally decorrelate slowly. In Fig. 9(c), $C^{+}_{\Delta I}$ for surface *B* exhibits essentially identical autocorrelation and reciprocal peaks, which overlap to produce a high central peak at the point for which both correlated intensities are at backscattering. Otherwise the decorrelation is rapid and strong; it appears that $C^{+}_{\Delta I}$ only rises where it must to produce the autocorrelation and reciprocal peaks. In the case of $C^{-}_{\Delta I}$, Fig. 9(b) shows that it is generally comparable to $C^{+}_{\Delta I}$ for surface *A* but, in Fig. 9(d), it is seen to be almost insignificant for surface *B*.

The decorrelation seen in $C^{+}_{\Delta I}$ for surface *B* may be made even more rapid by using a longer wave length, as is apparent with λ=674 nm in Fig. 10. In Fig. 10(d), for example, the width of the correlation peak of $C^{+}_{\Delta I}(k,k',\Delta_{qk})$ has narrowed to approximately 60% of the width of the result of Fig. 7(d). This observation will be discussed in Sec. V. Another notable difference is that the polariton coupling region

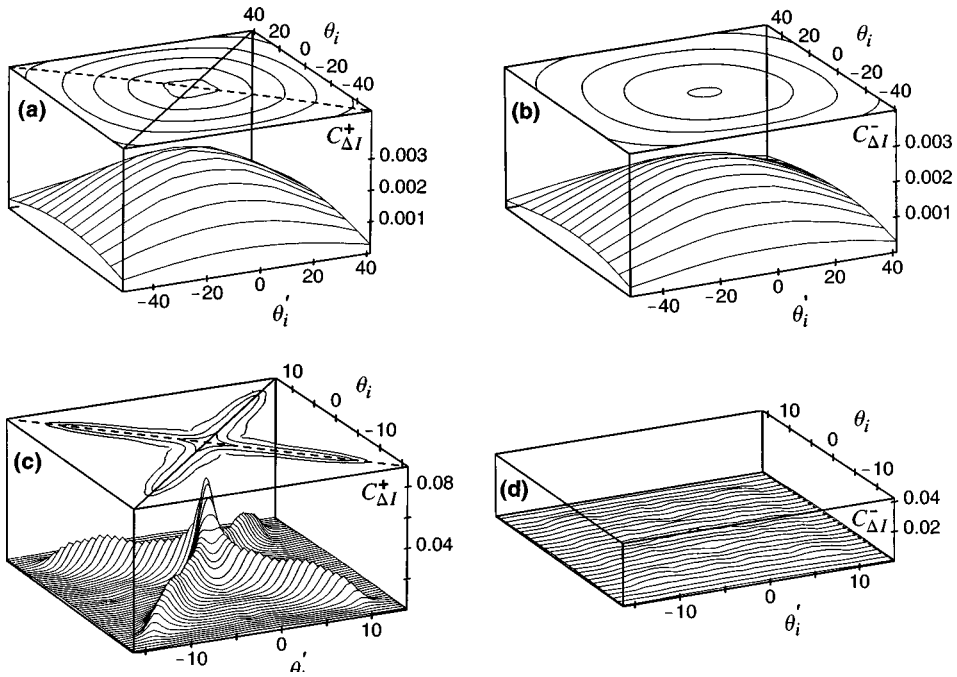

FIG. 9. Experimental results for $C^{\pm}_{\Delta I}(k,k',\Delta_{qk})$ of surface A [(a) and (b)] and surface B [(c) and (d)]. In $C^{+}_{\Delta I}$, solid- and dashed-diagonal lines follow the autocorrelation and reciprocal peaks, respectively. Units of $C^{\pm}_{\Delta I}$ are rad^{-2}, and θ_i and θ_i' are expressed in degrees.

has become wider in Fig. 10, but this had been seen previously in Fig. 4. Otherwise, Fig. 10 demonstrates that $C^{\pm}_{\Delta I}$ maintains much qualitative similarity to Fig. 7; the similarities also extend to $\rho^{\pm}_{\Delta I}$, although we do not show the latter measurements here.

A measure of the quality of the data is the degree of correlation at a reciprocal configuration expressed by $\rho^{+}_{\Delta I}(k,-k-\Delta_{qk},\Delta_{qk})$. It is expected that angular positioning errors could greatly reduce the reciprocal correlation. The average value of $\rho^{+}_{\Delta I}(k,-k-\Delta_{qk},\Delta_{qk})$ is 0.99 and 0.98 for surface B at with $\lambda=612$ and 674 nm, respectively, and is 0.97 for surface A. These values indicate that such errors were of little consequence.

Following the conventions of laser speckle theory,[31] we define the intensity contrast $\mathcal{C}$ as

$$\mathcal{C}=\frac{\sqrt{\langle I^2\rangle-\langle I\rangle^2}}{\langle I\rangle}. \tag{7}$$

A contrast of unity is consistent with the complex circular Gaussian amplitude statistics commonly assumed for well-developed speckle.[31] We find that the average $\mathcal{C}$ for our data sets is 1.00 and 1.01 for surface B with $\lambda=612$ and 674 nm, respectively, which is consistent with these amplitude statistics. However, for surface A the average contrast is only 0.95, but we do not attribute this to other amplitude statistics. Instead, the roughness of surface B is somewhat less one-dimensional than A; we observe that its speckle has a slight two-dimensional structure. Integrating this two-dimensional speckle over the length of the detection slit inevitably reduces $\mathcal{C}$, as generally occurs for integrated speckle.[31]

We now relate these observations to previous work. A correlation function like $C^{+}_{\Delta I}(k,k',\Delta_{qk})$ has appeared previously. For strongly rough surfaces, similar correlation functions of both amplitude and intensity that occur for $\Delta_{qk}=\Delta_{qk'}$ have been widely studied.[19–24] In the case of volume scattering,[27–29] the analogous intensity correlation is known as the memory effect; the reciprocal peak in this correlation was termed the time-reversed memory effect. For weakly rough surfaces,[15,16] $C^{+}_{\Delta I}$ has been called the $C^{(1)}$ correlation elsewhere, and $C^{-}_{\Delta I}$ has been termed the $C^{(10)}$ correlation. The above measurements are the first experimental observations of the latter correlation function.

It is equally important to note what correlation functions have not been observed in our experiments; these have been termed long-range correlations. To our knowledge, none of the following effects have ever been observed in surface scattering. One such correlation has been predicted to occur when $(q+k)=\pm(q'+k')$.[23] We have tried but failed to find statistically significant correlations in such cases. Another possibility is the $C^{(1.5)}$ correlation[15,16] that implies a correlation between the intensity of the single scatter and of the plasmon-polariton related scatter of surface B. We regret that the single scatter of surface B appears artificially non-Gaussian due to the discrete nature of the 500 exposures used in the fabrication; this sample is unsuitable for such measurements. Other polariton-related possibilities include the $C^{(2)}$ correlation,[15,16] which would, for example, predict six ridges at and near the lines $k=\pm k'$ in Fig. 9(d), but these are not present. Another is $C^{(3)}$, which predicts a correlation distributed throughout the entire speckle pattern,[15,16] yet we find no such effects. Using a narrower illumination region, which may make such correlations stronger, is impractical for us due to alignment difficulties.

IV. DISCUSSION

We now consider a fundamental question. Let us assume that the surface roughness is a statistically stationary random process and that the illuminated region is large. From these

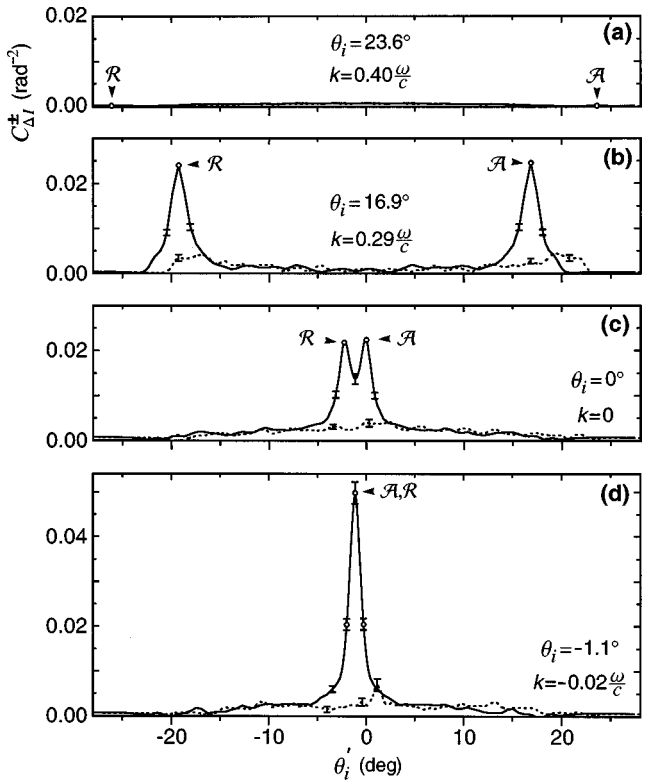

FIG. 10. Correlation functions $C^{+}_{\Delta I}(k,k',\Delta_{qk})$ (solid lines) and $C^{-}_{\Delta I}(k,k',\Delta_{qk})$ (dashed lines) for surface *B*, $\lambda = 674$ nm, and $\Delta_{qk} = 0.04\omega/c$. The autocorrelation ($\mathcal{A}$) and reciprocal ($\mathcal{R}$) peaks of $C^{+}_{\Delta I}$ have narrowed as compared to the case for $\lambda = 612$ nm in Fig. 7.

considerations alone, is it possible to determine what types of correlation functions of amplitude or intensity follow? Despite the wide variety of correlation functions discussed in Sec. III, the issue has not been adequately addressed previously. Nonetheless, our main conclusions are related to those of a number of previous works,[14–17] but this will be discussed in detail later. In our arguments that follow there are many subtleties; the discussion will stress plausibility at the expense of mathematical rigor.

Under these physical conditions, the far-field scattered amplitude arises from the sum of many independent contributions from different regions of the rough surface. As in speckle theory, we heuristically invoke the central limit theorem to conclude that the amplitude follows complex Gaussian statistics.[31] It has also been shown that, for a perfectly conducting rough surface, the scattered amplitude may be of nonvanishing mean only at the specular angle.[32] The proof relies only on the statistical stationarity of the surface source functions; we also expect this to be the case for the penetrable surface of interest here. We thus denote the diffusely scattered amplitude by $A(q|k)$, with it being understood that it has zero mean and that any specular reflection has been subtracted.

Consider now, for example, the intensity $I(q|k) = |A(q|k)|^2$. Making only the assumptions of the previous paragraph, it is readily shown that

$$\langle \Delta I(q|k)\Delta I(q'|k')\rangle = |\langle A(q|k)A^*(q'|k')\rangle|^2 + |\langle A(q|k)A(q'|k')\rangle|^2. \quad (8)$$

A moment theorem of the form of Eq. (8) has rarely been used elsewhere; it has been applied to the spatial speckle statistics of imaged phase screens.[33] In the vast majority of speckle work, the second term of Eq. (8) did not appear because of the additional assumption of circular statistics.[31,34,35] For the angular correlations, both terms must be retained. Further, we may make a stronger statement: The second-order moments $\langle A(q|k)A^*(q'|k')\rangle$ and $\langle A(q|k)A(q'|k')\rangle$ in Eq. (8) are fundamental because, for zero-mean Gaussian statistics, they *fully specify* the amplitude's statistical properties. Thus, all joint probability densities of amplitude immediately follow, and joint moments of arbitrary statistical order are guaranteed to follow from these amplitude moments.[34,35] Equation (8) is but a special case of the latter statement.

Our original question may thus be answered completely through accurate determination of the two amplitude moments. For this purpose, we employ the approach of Maradudin and Méndez[4] that, in each perturbation order, allows terms to be evaluated exactly. In this formulation, a *p*-polarized plane wave illuminates a long length L_1 of a surface with one-dimensional roughness. The diffuse amplitude is given by

$$A(q|k) = -i\left(\frac{2\pi}{L_1}\right)^{1/2} \mathcal{N}(\theta_i,\theta_s) G_0(q)\Delta T(q|k) G_0(k), \quad (9)$$

where $T(q|k)$ is the transition matrix, $\Delta T = T - \langle T\rangle$, and $G_0(k)$ is the plasmon polariton Green's function for a flat metal surface

$$G_0(k) = \frac{i\epsilon}{\epsilon\alpha_0(k) + \alpha(k)}, \quad (10)$$

where $\alpha_0(k) = \sqrt{(\omega/c)^2 - k^2}$ and $\alpha(k) = \sqrt{\epsilon(\omega/c)^2 - k^2}$. The factor

$$\mathcal{N}(\theta_i,\theta_s) = \left(\frac{\omega}{c}\right)^{3/2} \sqrt{\cos\theta_i}\,\frac{\cos\theta_s}{\pi} \quad (11)$$

guarantees that the mean diffuse intensity $\langle I(q|k)\rangle = \langle |A(q|k)|^2\rangle$ is normalized as in Figs. 2 and 4, as is seen from Eq. (3.4) of Ref. 4. The transition matrix is expanded into the perturbation series

$$T(q|k) = \sum_{n=1}^{\infty} \frac{(-i)^n}{n!} T^{(n)}(q|k) \quad (12)$$

where $T^{(n)}(q|k)$ is of order n in the surface profile function $\zeta(x)$. These terms may be cast as

$$T^{(1)}(q|k) = \mathcal{A}^{(1)}(q|k)\hat{\zeta}(q-k), \quad (13)$$

$$T^{(2)}(q|k) = \int_{-\infty}^{\infty} \frac{dp}{2\pi}\,\mathcal{A}^{(2)}(q|p|k)\hat{\zeta}(q-p)\hat{\zeta}(p-k), \quad (14)$$

$$T^{(3)}(q|k) = \int\int_{-\infty}^{\infty} \frac{dp}{2\pi}\frac{dr}{2\pi}\,\mathcal{A}^{(3)}(q|p|r|k) \times \hat{\zeta}(q-p)\hat{\zeta}(p-r)\hat{\zeta}(r-k), \quad (15)$$

and so on, where $\hat{\zeta}(k)$ is the Fourier transform of the surface profile

$$\hat{\zeta}(k)=\int_{-\infty}^{\infty} dx\,\zeta(x)\exp(-ikx). \tag{16}$$

The functions $\mathcal{A}^{(n)}$ are derived from the reduced Rayleigh equations and follow from the results of Ref. 4. For example,

$$\mathcal{A}^{(1)}(q|k)=i\,\frac{\epsilon-1}{\epsilon^2}\,[\epsilon qk-\alpha(q)\alpha(k)], \tag{17}$$

and an expression for $\mathcal{A}^{(3)}$ has appeared elsewhere.[10]

It is only necessary to insert Eqs. (12)–(15) into Eq. (9) and compute the two desired amplitude correlation functions. For convenience, we now assume that the surface profile $\zeta(x)$ is a real Gaussian process. Retaining terms to fourth order in σ, which is sufficient to obtain polariton-related effects,[4] we average over the statistics of $\zeta(x)$ to obtain

$$\begin{aligned}\langle A(q|k)A^*(q'|k')\rangle=&\left(\frac{2\pi}{L_1}\right)\mathcal{N}(\theta_i,\theta_s)\mathcal{N}(\theta_i',\theta_s')G_0(q)\\&\times G_0^*(q')\{\langle T^{(1)}(q|k)T^{(1)*}(q'|k')\rangle\\&+\tfrac{1}{4}\langle\Delta T^{(2)}(q|k)\Delta T^{(2)*}(q'|k')\rangle\\&-\tfrac{1}{6}\langle T^{(1)}(q|k)T^{(3)*}(q'|k')\rangle\\&-\tfrac{1}{6}\langle T^{(1)*}(q'|k')T^{(3)}(q|k)\rangle\}\\&\times G_0(k)G_0^*(k'),\end{aligned} \tag{18}$$

and

$$\begin{aligned}\langle A(q|k)A(q'|k')\rangle=&\left(\frac{2\pi}{L_1}\right)\mathcal{N}(\theta_i,\theta_s)\mathcal{N}(\theta_i',\theta_s')G_0(q)G_0(q')\\&\times\{\langle T^{(1)}(q|k)T^{(1)}(q'|k')\rangle\\&-\tfrac{1}{4}\langle\Delta T^{(2)}(q|k)\Delta T^{(2)}(q'|k')\rangle\\&-\tfrac{1}{6}\langle T^{(1)}(q|k)T^{(3)}(q'|k')\rangle\\&-\tfrac{1}{6}\langle T^{(1)}(q'|k')T^{(3)}(q|k)\rangle\}\\&\times G_0(k)G_0(k').\end{aligned} \tag{19}$$

The moments of Eq. (18) may be expressed as

$$\begin{aligned}\langle T^{(1)}(q|k)T^{(1)*}(q'|k')\rangle=&\,2\pi\sigma^2\delta[(q-k)-(q'-k')]\\&\times\mathcal{A}^{(1)}(q|k)\mathcal{A}^{(1)*}(q'|k')g(q-k),\end{aligned} \tag{20a}$$

$$\begin{aligned}&\langle\Delta T^{(2)}(q|k)\Delta T^{(2)*}(q'|k')\rangle\\&\quad=(2\pi\sigma^2)^2\delta[(q-k)-(q'-k')]\int_{-\infty}^{\infty}\frac{dp}{(2\pi)^2}\\&\qquad\times\mathcal{A}^{(2)}(q|p|k)\mathcal{S}_-^*(q,q',p,k')g(q-p)g(p-k),\end{aligned} \tag{20b}$$

and

$$\begin{aligned}\langle T^{(1)}(q|k)T^{(3)*}(q'|k')\rangle=&(2\pi\sigma^2)^2\delta[(q-k)-(q'-k')]\\&\times\mathcal{A}^{(1)}(q|k)\mathcal{H}^*(q'|k')g(q-k),\end{aligned} \tag{20c}$$

while those of Eq. (19) are given by

$$\begin{aligned}\langle T^{(1)}(q|k)T^{(1)}(q'|k')\rangle=&\,2\pi\sigma^2\delta[(q-k)+(q'-k')]\\&\times\mathcal{A}^{(1)}(q|k)\mathcal{A}^{(1)}(q'|k')g(q-k),\end{aligned} \tag{21a}$$

$$\begin{aligned}&\langle\Delta T^{(2)}(q|k)\Delta T^{(2)}(q'|k')\rangle\\&\quad=(2\pi\sigma^2)^2\delta[(q-k)+(q'-k')]\int_{-\infty}^{\infty}\frac{dp}{(2\pi)^2}\\&\qquad\times\mathcal{A}^{(2)}(q|p|k)\mathcal{S}_+(q,q',p,k')g(q-p)g(p-k),\end{aligned} \tag{21b}$$

and

$$\begin{aligned}\langle T^{(1)}(q|k)T^{(3)}(q'|k')\rangle=&(2\pi\sigma^2)^2\delta[(q-k)+(q'-k')]\\&\times\mathcal{A}^{(1)}(q|k)\mathcal{H}(q'|k')g(q-k).\end{aligned} \tag{21c}$$

Here $\delta[\,]$ denotes the Dirac delta function, $\mathcal{G}(k)=\sigma^2 g(k)$, and we have defined

$$\begin{aligned}\mathcal{S}_\pm(q,q',p,k')=&\,\mathcal{A}^{(2)}(q'|q'\pm q\mp p|k')\\&+\mathcal{A}^{(2)}(q'|k'\mp q\pm p|k'),\end{aligned} \tag{22}$$

and

$$\begin{aligned}\mathcal{H}(q|k)=&\int_{-\infty}^{\infty}\frac{dp}{(2\pi)^2}\,\mathcal{A}^{(3)}(q|p|q|k)g(q-p)+\int_{-\infty}^{\infty}\frac{dp}{(2\pi)^2}\\&\times[\mathcal{A}^{(3)}(q|k|p|k)+\mathcal{A}^{(3)}(q|q-k+p|p|k)]\\&\times g(p-k).\end{aligned} \tag{23}$$

In Eqs. (20) all contributions to $\langle A(q|k)A^*(q'|k')\rangle$ contain delta functions with argument $(q-k)-(q'-k')$, while Eqs. (21) for $\langle A(q|k)A(q'|k')\rangle$ contain delta functions in $(q-k)+(q'-k')$. This is not entirely surprising. It has been shown elsewhere that, for a perfectly conducting rough surface, the statistical stationarity of the surface source function restricts the correlation $\langle A(q|k)A^*(q'|k')\rangle$ to the condition noted.[21] We expect that similar stationarity arguments should apply to penetrable surfaces. Further, in extending the approach of Ref. 21 to the unconjugated correlation $\langle A(q|k)A(q'|k')\rangle$, it is straightforward to show that the restriction to $(q-k)=-(q'-k')$ follows directly. It is thus highly plausible that, for any statistically stationary roughness, the delta functions present in either Eqs. (20) or (21) persist throughout terms of arbitrary order.

Thus, $\langle A(q|k)A^*(q'|k')\rangle$ and $\langle A(q|k)A(q'|k')\rangle$ usually appear distinctly; in particular, when $(q-k)=(q'-k')$ the former moment is nonzero but the latter vanishes, and the situation is reversed for $(q-k)=-(q'-k')$. Both of these correlations are of the short-range type, arising as delta functions in q and k. Indeed, the approach taken here has appar-

ently excluded all long-range correlations; these have strengths proportional to the inverse of the illumination width[15,16] and should thus be absent in the limit taken here. Still, our assumption of plane-wave illumination differs from the Gaussian beam of the experiments, but the consequences of such differences should be small. In the case of $\langle A(q|k)A^*(q'|k')\rangle$, it has been shown that the amplitude correlation function with beam illumination is nearly identical to that with a plane wave, as long as the beam has a diffraction width much narrower than the structure in $\langle A(q|k)A^*(q'|k')\rangle$;[21] an analogous conclusion has also been reached from direct studies of the intensity correlation function.[16] This condition seems satisfied in the experiments; with $\lambda=612$ nm, for example, the full width at half maximum of the intensity of the incident beam is 0.28°, which is far less than the 2.4° width of $C_{\Delta I}^{+}$ in Fig. 7(d).

We now relate our approach to those taken elsewhere. Reference 14 was unaware of the second term of Eq. (8), and evaluated the first term with a perturbation theory of a different type. In Refs. 15 and 16, perturbation theory was developed for the full intensity correlation with the surface illuminated by a beam of Gaussian profile. Here, to leading order in σ, the moment theorem of Eq. (8) can be seen to be valid and the results exhibit appropriate delta functions with arguments $(q-k)\pm(q'-k')$. However, in higher-order terms, the long-range correlations contribute and Eq. (8) no longer applies. Nevertheless, in the limit of large illumination width the long-range effects should vanish and Eq. (8) should be recovered, but this is not obvious due to the complexity of the theory.

In Ref. 17 the noncircular moment theorem of Eq. (8) was indeed originally proposed for the angular correlation functions. From numerical simulations of scattering from a statistical ensemble of rough surfaces, the intensity correlation function was calculated by averaging over this ensemble. It was thus shown that the two terms of Eq. (8) contributed distinctly, in the same manner as discussed above. For a rectangular spectrum $\mathcal{G}(k)$, it was found that the scattered amplitude was highly non-Gaussian, having speckle contrast $\mathcal{C}$ that deviated 70% from unity, and that the long-range correlations were several times stronger than $C_{\Delta I}^{\pm}(k,k',\Delta_{qk})$. It is unclear why these claims are different from the results of our controlled experiments with surface *B* in Sec. III, where $\mathcal{C}$ was essentially unity and the long-range correlations were absent. It was also claimed that the moment theorem of Eq. (8) does not affect the speckle contrast $\mathcal{C}$. In Sec. V, we give several examples in which there may be significant effects on $\mathcal{C}$.

While the circular moment theorem [i.e., Eq. (8) with the second term absent] has sometimes been referred to as a factorization approximation, this name may be misleading. Indeed, here we have made one different approximation: that the amplitude follows complex Gaussian statistics. It is then only an exercise to determine, from physical principles, all amplitude moments of first and second statistical order, thus specifying all parameters of the Gaussian probability distribution. At this point the problem is as good as solved; any required statistical moment follows immediately from the distribution. This approach thus leads directly to Eq. (8) and there is no violation of a factorization approximation.

V. NUMERICAL RESULTS

Here we present results based on numerical integration of the expressions from Sec. IV. The divergence from the delta functions of Eqs. (20) and (21) is artificial and arises from treating the profile $\zeta(x)$ as having infinite length. To evaluate $\langle A(q|k)A^*(q'|k')\rangle$ and $\langle A(q|k)A(q'|k')\rangle$ from Eqs. (18)–(21), we have thus transformed factors as

$$\left(\frac{2\pi}{L_1}\right)\delta[(q-k)-(q'-k')]\rightarrow\delta_{(q-k),(q'-k')} \tag{24a}$$

and

$$\left(\frac{2\pi}{L_1}\right)\delta[(q-k)+(q'-k')]\rightarrow\delta_{(q-k),-(q'-k')}, \tag{24b}$$

where subscripted deltas are of the Kronecker type; these are analogous to Eq. (4.1) of Ref. 4. The amplitude correlations are nonzero but finite as determined by the arguments of the Kronecker delta functions, and results may thus be expressed as

$$C_A^{+}(k,k',\Delta_{qk})=\langle A(k+\Delta_{qk}|k)A^*(k'+\Delta_{qk}|k')\rangle \tag{25}$$

and

$$C_A^{-}(k,k',\Delta_{qk})=\langle A(k+\Delta_{qk}|k)A(k'-\Delta_{qk}|k')\rangle, \tag{26}$$

that are similar to Eqs. (4) and (5). We also define the statistically normalized correlation functions

$$\rho_A^{\pm}(k,k',\Delta_{qk})=\frac{C_A^{\pm}(k,k',\Delta_{qk})}{\sqrt{\langle|A(q|k)|^2\rangle\langle|A(q'|k')|^2\rangle}}, \tag{27}$$

with $0\leqslant|\rho_A^{\pm}|\leqslant1$, where $\langle|A(q|k)|^2\rangle$ follows as a special case of Eq. (18).

In calculations for surface *A*, we have employed the spectrum

$$g(k)=\frac{2b\ \exp(-a^2/b^2)}{1-\mathrm{erf}(a/b)}\,\frac{\exp(-k^2a^2)}{1+k^2b^2}. \tag{28}$$

This model agrees closely with the experimental spectrum as is seen in Fig. 1; a least-squares fit has provided the parameters $a=89$ nm and $b=190$ nm. We show results for surface *A* in Fig. 11, assuming the dielectric constant of gold to be $\epsilon=-9.0+1.29i$ for $\lambda=612$ nm. The two amplitude correlation functions show a broad angular structure and are dominated by the 1-1 terms of Eqs. (18) and (19); the 1-3 terms make contributions of similar shape but are approximately one order of magnitude smaller. It is seen that $C_A^{+}(k,k',\Delta_{qk})$ is largely real and positive, while $C_A^{-}(k,k',\Delta_{qk})$ is dominated by a negative imaginary part. There are peaks at the autocorrelation and reciprocal positions in $\mathrm{Re}[C_A^{+}]$ that are hardly discernible; they arise from a small 2-2 contribution from Eq. (20b). Most of decay of $|C_A^{\pm}|$ arises from the fall of the mean intensity and there is little actual decorrelation; we find that $|\rho_A^{\pm}|>0.93$ throughout Fig. 11, although we do not show results for $\rho_A^{\pm}$ here.

These calculations may be readily compared with the experimental results of Sec. III. In particular, it follows directly from earlier discussions that $C_{\Delta I}^{\pm}(k,k',\Delta_{qk})$

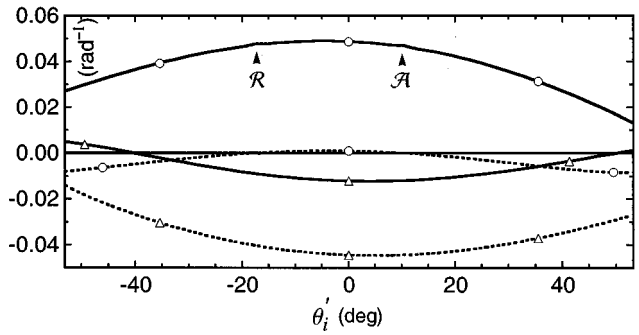

FIG. 11. Calculated amplitude correlation functions $C_A^+(k,k',\Delta_{qk})$ (circles) and $C_A^-(k,k',\Delta_{qk})$ (triangles) for the spectrum of Eq. (28) with $\lambda=612$ nm, $\epsilon=-9.0+1.29i$, $\Delta_{qk}=0.12\omega/c$, and $k=0.18\omega/c$. Solid and dashed lines denote, respectively, the real and imaginary parts. Autocorrelation ($\mathcal{A}$) and reciprocal ($\mathcal{R}$) points are indicated.

$=|C_A^{\pm}(k,k',\Delta_{qk})|^2$ and $\rho_{\Delta I}^{\pm}(k,k',\Delta_{qk})=|\rho_A^{\pm}(k,k',\Delta_{qk})|^2$. We show such comparisons for surface A in Fig. 12. We had pointed out in Sec. III that the experimental contrast $\mathcal{C}$ was 0.95 because of surface defects; we have crudely corrected for this by scaling $|C_A^{\pm}|^2$ by the factor $\mathcal{C}^2$. There are otherwise no free parameters and the agreement between $C_{\Delta I}^{\pm}$ and $|C_A^{\pm}|^2$ in Fig. 12(a) is thus remarkably good. In the comparison between the calculated $|\rho_A^+|^2$ and the experimental $\rho_{\Delta I}^+$ in Fig. 12(b), both results share peaks at the autocorrelation and reciprocal points, but the latter decays more rapidly for large $|\theta_i'|$. It is seen that $|\rho_A^-|^2$ and $\rho_{\Delta I}^-$ show somewhat less correlation, with the experimental curve being lower. Including terms only to order σ^2, it is straightforward to show that $|\rho_A^{\pm}|=1$; thus the fourth-order terms are required to produce decorrelation. It may require yet higher-order perturbation terms to predict further decorrelation, so as to be more similar to the experimental results.

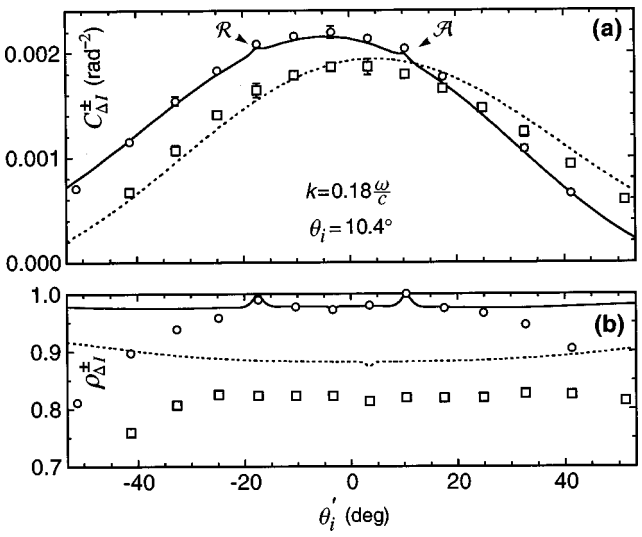

FIG. 12. Results for surface A, $\lambda=612$ nm, $\Delta_{qk}=0.12\omega/c$, and $k=0.18\omega/c$. Top: Measurements of $C_{\Delta I}^+$ (circles) and $C_{\Delta I}^-$ (squares) are compared with calculations of $|C_A^+|^2$ (solid curve) and $|C_A^-|^2$ (dotted curve). Bottom: Measurements of $\rho_{\Delta I}^+$ (circles) and $\rho_{\Delta I}^-$ (squares) are compared with calculations of $|\rho_A^+|^2$ (solid curve) and $|\rho_A^-|^2$ (dotted curve).

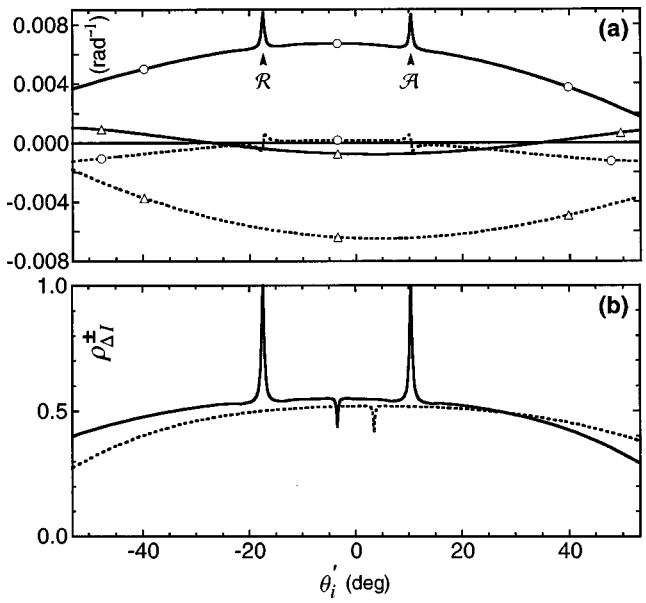

FIG. 13. Results for the Gaussian spectrum of Eq. (29) with $\lambda=457.9$ nm, $\epsilon=-7.5+0.24i$, $\Delta_{qk}=0.12\omega/c$, and $k=0.18\omega/c$. Top: Calculations of C_A^+ (circles) and C_A^- (triangles); solid and dotted lines denote, respectively, the real and imaginary parts. Bottom: Calculations of $|\rho_A^+|^2$ (solid line) and $|\rho_A^-|^2$ (dotted line); the autocorrelation ($\mathcal{A}$) and reciprocal ($\mathcal{R}$) peaks in $|\rho_A^+|^2$ imply perfect correlation.

We next consider the case of the Gaussian spectrum

$$g(k)=\sqrt{\pi}a\ \exp(-k^2a^2/4). \tag{29}$$

To be consistent with theoretical works studying backscattering enhancement for this surface model,[1,4,11] we assume $a=100$ nm, $\sigma=5$ nm, $\lambda=457.9$ nm, and $\epsilon=-7.5+0.24i$. It is expected that the plasmon polariton excitation will be more apparent; $g(k_{sp})/g(0)$ is eight times higher than for surface A. However, no experimental studies of this surface have appeared because of fabrication difficulties that we also cannot surmount.

Results for $C_A^{\pm}(k,k',\Delta_{qk})$ are shown for the Gaussian spectrum in Fig. 13(a); the results are of lower scale than Fig. 11 because of the reduction in σ. The broad features resemble the results for surface A and arise similarly from the 1-1 and 1-3 terms. However, there are now distinct peaks in $\mathrm{Re}[C_A^+]$ that appear at the autocorrelation and reciprocal points. These arise entirely from the 2-2 term, as do the associated zero crossings in $\mathrm{Im}[C_A^+]$. No such structures are seen in C_A^- and we find that its 2-2 term makes a small, featureless contribution. In Fig. 13(b), we also show the correlation functions $|\rho_A^{\pm}(k,k',\Delta_{qk})|^2$ that indicate a substantial decorrelation of the speckle intensity. There are distinct minima that appear as the normalization factor $\langle|A(q'|k')|^2\rangle$ in Eq. (27) passes through its backscattering peak. In $|\rho_A^+|^2$, there are narrow autocorrelation and reciprocal peaks where the correlation is perfect; these also arise from the 2-2 contribution to C_A^+.

We now consider the case of an ideal rectangular spectrum for which $g(k)$ has constant height for $k_{\min}\leqslant|k|\leqslant k_{\max}$, with $g(k)=0$ for all other k. Using the parameters of surface B we find that, keeping terms of up to fourth order,

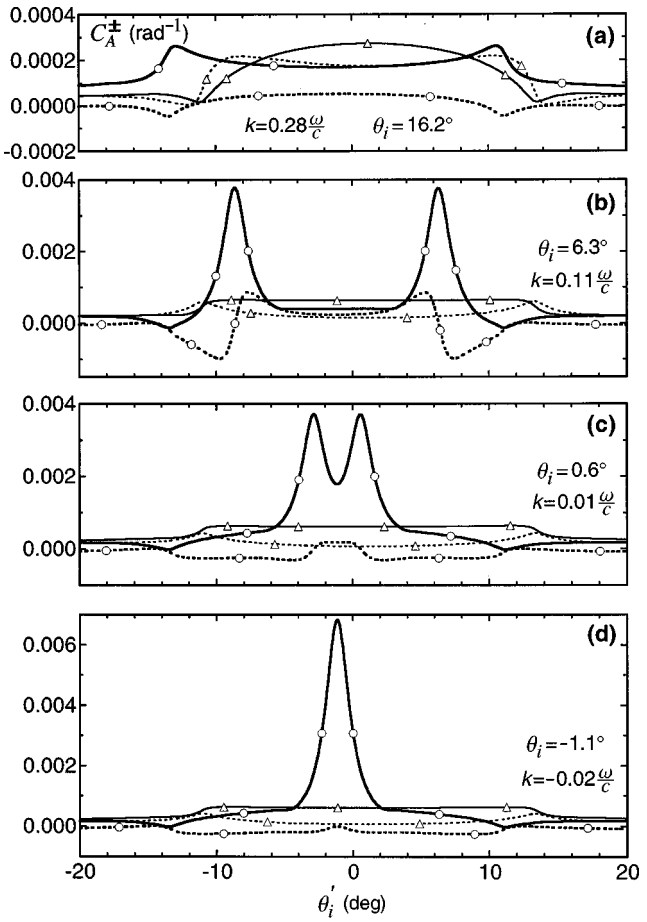

FIG. 14. Calculations for the case of the ideal rectangular spectrum with $\sigma=5$ nm, $\lambda=612$, $\epsilon=-9.0+1.29i$, and $\Delta_{qk}=0.04\omega/c$. Shown are $C_A^+(k,k',\Delta_{qk})$ (circles) and $C_A^-(k,k',\Delta_{qk})$ (triangles); solid and dashed lines denote, respectively, the real and imaginary parts.

the predicted diffuse intensity in the polariton-coupling region is twice that of the experimental results of Figs. 2 and 4. This is evidence that the surface is too rough for direct comparison with perturbation theory of this order. We thus present numerical results for a weaker (and fictitious) surface, and confine the discussion to qualitative experimental comparisons. In the calculations, we assume the surface to have an ideal rectangular spectrum with $k_{\min}$ and $k_{\max}$ as in Sec. II, $\sigma=5.0$ nm, $\lambda=612$ nm, and $\epsilon=-9.0+1.29i$.

The results for $C_A^{\pm}(k,k',\Delta_{qk})$ are shown for $\Delta_{qk}=0.04\omega/c$ in Fig. 14 and exhibit much similarity to the experimental results of Fig. 7. It is notable that $C_A^{\pm}$ arises solely from the 2-2 terms; contributions from all other terms of Eqs. (20) and (21) vanish because of the common factor $g(q-k)$, which is zero under the conditions of Fig. 14. Peaks similar to those in $C_{\Delta I}^+(k,k',\Delta_{qk})$ of Fig. 7 appear in $\mathrm{Re}[C_A^+]$ and related structures are seen in $\mathrm{Im}[C_A^+]$. As had been the case for $C_{\Delta I}^-$ in Fig. 7, C_A^- remains small throughout Fig. 14; its levels are comparable to those of C_A^+ in Fig. 14(a). There are, however, subtle differences in comparisons with experimental data. The peak width (the full width at half maximum) of, for example, $C_{\Delta I}^+$ in Fig. 7(d) is 2.4° while, upon taking $|C_A^+|^2$ from the result of Fig. 14(d), we find a peak width of only 1.4°. This difference may arise from the radiative damping of plasmon polaritons[1] on the strong experimental surface or, as will be seen, from differences between the assumed and actual values of ϵ. Finally, we note that our calculations for $|\rho_A^{\pm}(k,k',\Delta_{qk})|^2$ for the rectangular spectrum bear much qualitative similarity to the experimental results of Fig. 8, even to the point of resembling the unusual forms of Fig. 8(a), but we do not show these results here.

We claim that the peaks of $C_A^+(k,k',\Delta_{qk})$ seen throughout results arise from processes that are generalizations of those producing backscattering enhancement. This may be shown through approximate evaluation of the 2-2 contribution to C_A^+. For this purpose, we write

$$\mathcal{A}^{(2)}(q|p|k)\cong 2\mathcal{A}^{(1)}(q|p)G_0(p)\mathcal{A}^{(1)}(p|k), \tag{30}$$

which neglects terms that make small contributions. This simplification is made in Eqs. (20b) and (22), and the products of displaced Green's functions may be treated with a pole approximation[4]

$$G_0(p)G_0^*(x-p)\cong \frac{2\pi i C^2}{2i\Delta_\epsilon - x}\,\delta(p-k_{sp}) + \frac{2\pi i C^2}{2i\Delta_\epsilon + x}\,\delta(p+k_{sp}), \tag{31}$$

where

$$C_\epsilon=\frac{|\epsilon_1|^{3/2}}{\epsilon_1^2-1} \tag{32}$$

and

$$\Delta_\epsilon=\tfrac{1}{2}\epsilon_2\,\frac{k_{sp}}{|\epsilon_1|[|\epsilon_1|-1]}. \tag{33}$$

Upon performing the integral we obtain, to an excellent approximation,

$$\begin{aligned}\langle \Delta T^{(2)}(q|k)\Delta T^{(2)*}(q'|k')\rangle &= 2L_1\sigma^4 C_\epsilon^2\delta_{(q-k),(q'-k')}\Bigg\{\frac{2i}{2i\Delta_\epsilon-(k-k')}\\ &\times F_+(q|k)F_+^*(q'|k')g(q-k_{sp})g(k_{sp}-k)\\ &+\frac{2i}{2i\Delta_\epsilon-(q+k')}\,F_+(q|k)F_-^*(q'|k')g(q-k_{sp})\\ &\times g(k_{sp}-k)+\frac{2i}{2i\Delta_\epsilon+(q+k')}\,F_-(q|k)F_+^*\\ &\times(q'|k')g(q+k_{sp})g(-k_{sp}-k)+\frac{2i}{2i\Delta_\epsilon+(k-k')}\\ &\times F_-(q|k)F_-^*(q'|k')g(q+k_{sp})g(-k_{sp}-k)\Bigg\},\end{aligned} \tag{34}$$

where $F_\pm(q|k)=\mathcal{A}^{(1)}(q|\pm k_{sp})\mathcal{A}^{(1)}(\pm k_{sp}|k)$ represents the coupling of an incident state k to a scattered state q, via the plasmon polariton $\pm k_{sp}$.

For the ideal rectangular spectrum, we employ the approximate 2-2 term of Eq. (34) to evaluate $C_A^+(k,k',\Delta_{qk})$ in

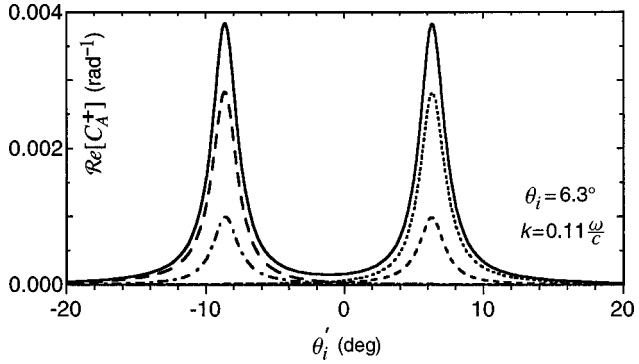

FIG. 15. From the pole approximation, the contributions to $\mathrm{Re}[C_A^+(k,k',\Delta_{qk})]$ from Eq. (34) for the ideal rectangular spectrum. The autocorrelation peak (right) contains contributions from the first term (dashed curve) and last term (dotted curve) of Eq. (34); the reciprocal peak (left) shows contributions from the second (dot-dashed curve) and third terms (broadly dashed curve). The solid curve indicates the total.

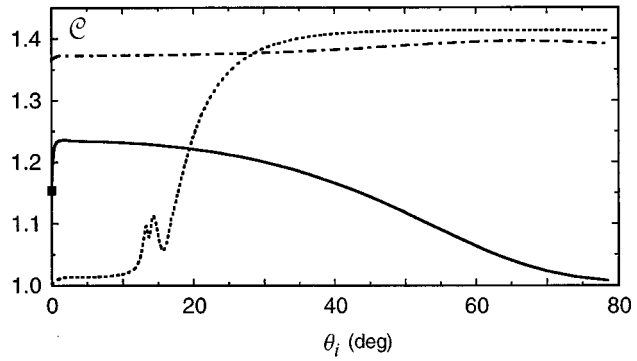

FIG. 16. The calculated intensity contrast $\mathcal{C}$ at specular for the model of surface A (dot-dashed curve), the Gaussian spectrum (solid curve), and the ideal rectangular spectrum (dotted curve).

Fig. 15; the 1-1 and 1-3 contributions here vanish. The results are quite similar to those obtained in Fig. 14(b) from exact numerical integration. Further, the contributions of the four terms of Eq. (34) are plotted distinctly and reveal structures that may be interpreted as arising from interference between scattering processes. The first and fourth terms of Eq. (34) represent interference terms between the processes $k \rightarrow \pm k_{sp} \rightarrow q$ and $k' \rightarrow \pm k_{sp} \rightarrow q'$. In Fig. 15, these processes interfere constructively to contribute to the autocorrelation peak at $k' = k$. The reciprocal peak arises from the second and third terms of Eq. (34). The second term represents the interference between processes $k \rightarrow +k_{sp} \rightarrow q$ and $k' \rightarrow -k_{sp} \rightarrow q'$. The latter process becomes a time-reversed version of the former at a reciprocal configuration with $(q',k') = (-k,-q)$, thus producing the reciprocal peak. A similar argument applies to the third term of Eq. (34), which expresses the interference between $k \rightarrow -k_{sp} \rightarrow q$ and $k' \rightarrow +k_{sp} \rightarrow q'$. Previously, related arguments have been applied to multiple scattering from a strongly rough metal surface,[22] but the intermediate state is not a plasmon polariton.

The backscattering peak in the mean intensity of Figs. 2 and 4 is also a consequence of this interference. It arises for $q = -k = q' = -k'$ where all four processes are correlated; the four terms of Eq. (34) produce equal and simultaneous contributions to this peak. Thus, $C_A^+(k,k',\Delta_{qk})$ has allowed us to see more distinctly the contributions that produce the backscattering peak. Further, it is remarkable that the peaks occur when both (q,k) and (q',k') are far from backscattering in Fig. 15, but these coherent processes make distinct contributions nonetheless. The results also indicate that the amplitude arising via the polariton-related processes decorrelates rapidly; such rapid decorrelation is not associated with the scattering processes contained in the 1-1 or 1-3 terms. It is readily shown from Eq. (34) that the width (full width at half maximum) of either peak in $\mathrm{Re}[C_A^+(k,k',\Delta_{qk})]$ or $|C_A^+(k,k',\Delta_{qk})|^2$ is given by $\Delta k' = 4\Delta_\epsilon$. In terms of θ_i', this implies widths of $\Delta\theta_i' = 4c\Delta_\epsilon/(\omega \cos\theta_i)$ and $\Delta\theta_i' = 4c\Delta_\epsilon/(\omega \cos\theta_s)$ for the autocorrelation and reciprocal peaks, respectively. These arguments apply directly to peak widths for surface B, or else to the peak width above the background when there are significant 1-1 and 1-3 contributions. It had been noted in Sec. III that the peaks were narrower for $\lambda = 674$ nm than 612 nm; this trend is consistent with the behavior of Δ_ϵ as ϵ_1 changes rapidly with λ.[36]

Finally, we consider effects on the speckle contrast $\mathcal{C}$ of Eq. (7). The variance of the intensity follows from Eq. (8) with $(q,k) = (q',k')$. Assuming that $\Delta_{qk} \neq 0$, the delta functions noted in Sec. IV guarantee that the second term of Eq. (8) vanishes so that $\langle \Delta I^2 \rangle = \langle I \rangle^2$. Thus $\mathcal{C}$ is constrained to unity, as would have been the case for circular Gaussian statistics. This conclusion is consistent with the experimental results of Sec. III where $\mathcal{C} \cong 1$. However, for the special case at specular with $q = k = q' = k'$, both terms of Eq. (8) contribute so that

$$\mathcal{C} = \frac{\sqrt{\langle I \rangle^2 + |\langle A^2 \rangle|^2}}{\langle I \rangle}, \tag{35}$$

and it is clear that $\mathcal{C}$ may exceed unity. At specular, this definition of $\mathcal{C}$ is slightly different from that often employed[31] because the mean amplitude was subtracted to define $A(q|k)$ in Sec. IV. However, the mean-specular amplitude is infinite in this theory and its subtraction is necessary to obtain a nonvanishing $\mathcal{C}$.

The specular contrast was evaluated from numerical integration of Eqs. (18) and (19) to determine $\langle I \rangle$ and $\langle A^2 \rangle$, respectively. Figure 16 shows the results for the same parameters used earlier for surface A, the Gaussian model, and the ideal rectangular spectrum. It is seen that surface A produces a contrast of nearly 1.4, with a shallow minimum at $\theta_i = 0°$ as the intensity passes through backscattering. The Gaussian model has nearly unit contrast for large θ_i, but $\mathcal{C}$ rises above 1.2 for smaller θ_i, only to fall to 1.15 at backscattering. The contrast for the rectangular spectrum is similar to surface A for large θ_i but falls to less than 1.02 for $\theta_i < 11°$, and falls further to $\mathcal{C} \cong 1$ at $\theta_i = 0°$. These results suggest that polariton-related scattering contributions tend to reduce the contrast; this is most clear from the abrupt fall of contrast, either for the rectangular spectrum for small θ_i, or for all three cases at backscattering. For a Gaussian-like spectrum, a substantial increase in σ will produce stronger polariton coupling and may then drive the specular contrast toward unity. However, a thorough investigation of this speculation would require a more complete theory than the low-order terms employed here.

VI. CONCLUSIONS

We have presented a detailed investigation of the angular correlation functions for *p*-polarized light scattered from weakly rough metal surfaces. In experimental work, we have used sophisticated fabrication techniques to produce two randomly rough surfaces with different power spectra. For the first surface, there is little plasmon polariton excitation and the correlation function $C_{\Delta I}^{+}(k,k',\Delta_{qk})$ indicates that the intensity decorrelates slowly as the angle of incidence is varied. Further, $C_{\Delta I}^{-}(k,k',\Delta_{qk})$ is strong and demonstrates that the scattered intensity, although random, possesses somewhat symmetric structure about the specular direction. In the case of the second surface, plasmon polariton excitation is significant and the behavior is strikingly different; $C_{\Delta I}^{+}$ indicates that the intensity decorrelates extremely rapidly, and $C_{\Delta I}^{-}$ remains quite small, so that the symmetry is nearly absent. Under our experimental conditions, these two correlation functions are all that are observed, and long-range correlations seem to be below statistical noise levels.

It has also been shown that the statistical properties of the scattered light are fully specified by the amplitude correlation functions $C_{A}^{+}(k,k',\Delta_{qk})$ and $C_{A}^{-}(k,k',\Delta_{qk})$, and that a rarely-used Gaussian moment theorem relates these directly to $C_{\Delta I}^{+}$ and $C_{\Delta I}^{-}$. These conclusions are based on plausibility arguments that appear to be valid for statistically stationary roughness in the limit of large illuminated area. Using a perturbation approach exact to fourth order in the surface profile, C_{A}^{+} and C_{A}^{-} have been evaluated, and comparisons with experimental results for $C_{\Delta I}^{+}$ and $C_{\Delta I}^{-}$ are generally favorable. This theoretical approach is less sophisticated than others employed to investigate long-range correlations, yet it is fully capable of reproducing all essential features of our experimental results. Further, should the fourth-order theory be inadequate, it is only necessary to find another means of calculating C_{A}^{+} and C_{A}^{-}, which may be a far less formidable task than the direct calculation of $C_{\Delta I}^{+}$ and $C_{\Delta I}^{-}$.

It has been discussed that C_{A}^{+} and C_{A}^{-} both express perfect correlation for scatter consistent with lowest-order perturbation theory but, as higher-order terms become significant, their behavior differs. When there is significant plasmon polariton excitation, C_{A}^{+} presents peaks that arise from coherent mechanisms identical to those producing backscattering enhancement. Further, C_{A}^{+} must remain important even as the roughness is increased to arbitrary levels; at the least, it must rise to express perfect correlation for its autocorrelation and reciprocal peaks. In the case of C_{A}^{-}, however, we have found that higher-order perturbation terms reduce the degree of correlation implicit throughout C_{A}^{-}. In addition, we have not found peaks within C_{A}^{-} that arise from coherent mechanisms, even under conditions for which such peaks are present in C_{A}^{+}. Although C_{A}^{-} is, in principle, always present for any rough surface, its behavior and significance for stronger roughness remain open issues.

ACKNOWLEDGMENT

We are grateful for discussions with E. R. Méndez.

*Present address: Optical Sciences Division, Naval Research Laboratory, 4555 Overlook Ave. SW, Washington, D.C. 20375.

†Present address: Division de Fisica Aplicada, Centro de Investigación Científica y de Educación Superior de Ensenada, Ensenada, Baja California, Mexico.

[1] A. R. McGurn, A. A. Maradudin, and V. Celli, Phys. Rev. B **31**, 4866 (1985); V. Celli, A. A. Maradudin, A. M. Marvin, and A. R. McGurn, J. Opt. Soc. Am. A **2**, 2225 (1985).

[2] A. R. McGurn and A. A. Maradudin, J. Opt. Soc. Am. A **4**, 910 (1987).

[3] V. Freilikher and I. Yurkevich, Phys. Lett. A **183**, 247 (1993); **183**, 253 (1993).

[4] A. A. Maradudin and E. R. Méndez, Appl. Opt. **32**, 3335 (1993).

[5] A. A. Maradudin, A. R. McGurn, and E. R. Méndez, J. Opt. Soc. Am. A **12**, 2500 (1995).

[6] H. Ogura and Z. L. Wang, Phys. Rev. B **53**, 10 358 (1996).

[7] M. Arnold and A. Otto, Opt. Commun. **125**, 122 (1996).

[8] A. R. McGurn and A. A. Maradudin, Waves Random Media **6**, 251 (1996).

[9] H. Hanato, H. Ogura, and Z. L. Wang, Waves Random Media **7**, 11 (1997).

[10] K. A. O'Donnell, C. S. West, and E. R. Méndez, Phys. Rev. B **57**, 13 209 (1998).

[11] P. Tran and V. Celli, J. Opt. Soc. Am. A **5**, 1635 (1988); T. R. Michel, *ibid.* **11**, 1874 (1994).

[12] C. S. West and K. A. O'Donnell, J. Opt. Soc. Am. A **12**, 390 (1995).

[13] C. S. West and K. A. O'Donnell, Opt. Lett. **21**, 1 (1996).

[14] A. Arsenieva and S. Feng, Phys. Rev. B **47**, 13 047 (1993).

[15] V. Malyshkin, A. R. McGurn, T. A. Leskova, A. A. Maradudin, and M. Nieto-Vesperinas, Opt. Lett. **22**, 946 (1997).

[16] V. Malyshkin, A. R. McGurn, T. A. Leskova, A. A. Maradudin, and M. Nieto-Vesperinas, Waves Random Media **7**, 479 (1997).

[17] M. Nieto-Vesperinas, A. A. Maradudin, A. V. Shchegrov, and A. R. McGurn, Opt. Commun. **142**, 1 (1997).

[18] E. Archbold and A. E. Ennos, Opt. Acta **19**, 253 (1972).

[19] H. M. Pedersen, Opt. Acta **22**, 523 (1975).

[20] D. Léger and J. C. Perrin, J. Opt. Soc. Am. **66**, 1210 (1976).

[21] T. R. Michel and K. A. O'Donnell, J. Opt. Soc. Am. A **9**, 1374 (1992).

[22] M. E. Knotts, T. R. Michel, and K. A. O'Donnell, J. Opt. Soc. Am. A **9**, 1822 (1992).

[23] M. Nieto-Vesperinas and J. A. Sánchez-Gil, Phys. Rev. B **46**, 3112 (1992); J. Opt. Soc. Am. A **10**, 150 (1993).

[24] Y. Kuga, C. T. C. Le, A. Ishimaru, and L. Ailes-Sengers, IEEE Trans. Geosci. Remote Sens. **34**, 1300 (1996).

[25] Y. Kuga and A. Ishimaru, J. Opt. Soc. Am. A **1**, 831 (1984).

[26] M. P. van Albada and A. Lagendijk, Phys. Rev. Lett. **55**, 2692 (1985); P. E. Wolf and G. Maret, *ibid.* **55**, 2696 (1985).

[27] S. Feng, C. Kane, P. A. Lee, and A. D. Stone, Phys. Rev. Lett. **61**, 834 (1988).

[28] R. Berkovits, M. Kaveh, and S. Feng, Phys. Rev. B **40**, 737 (1989); R. Berkovits and M. Kaveh, *ibid.* **41**, 2635 (1990); I. Freund and R. Berkovits, *ibid.* **41**, 496 (1990); L. Wang and S. Feng, *ibid.* **40**, 8284 (1989).

[29] I. Freund, M. Rosenbluh, and S. Feng, Phys. Rev. Lett. **61**, 2328 (1988); I. Freund, M. Rosenbluh, and R. Berkovits, Phys. Rev. B **39**, 12 403 (1989); N. Garcia and A. Z. Genack, Phys. Rev. Lett.

63, 1678 (1989); M. P. van Albada, J. F. de Boer, and A. Lagendijk, *ibid.* **64**, 2787 (1990); I. Freund and M. Rosenbluh, Opt. Commun. **82**, 362 (1991).
[30] D. S. Saxon, Phys. Rev. **100**, 1771 (1955).
[31] J. W. Goodman, in *Laser Speckle and Related Phenomena*, 2nd ed., edited by J. C. Dainty (Springer-Verlag, New York, 1984), pp. 9–75.
[32] G. S. Brown, IEEE Trans. Antennas Propag. **AP-30**, 1135 (1982).
[33] H. M. Pedersen, Opt. Commun. **16**, 63 (1976); B. Stoffregen, Optik (Stuttgart) **52**, 305 (1978); **52**, 385 (1978); E. R. Méndez, Opt. Acta **32**, 209 (1985).
[34] J. W. Goodman, *Statistical Optics* (Wiley, New York, 1985), pp. 108 and 109.
[35] B. Saleh, *Photoelectron Statistics* (Springer-Verlag, Berlin, 1978), pp. 38–40.
[36] D. W. Lynch and W. R. Hunter, in *Handbook of Optical Constants of Solids*, edited by Edward D. Palik (Academic, New York, 1985), p. 294.